MODERATE C IV ABSORBER SYSTEMS REQUIRE 10^{12} $M_\odot$ DARK MATTER HALOS AT $z \sim 2.3$: A CROSS-CORRELATION STUDY OF C IV ABSORBER SYSTEMS AND QUASARS IN SDSS-III BOSS DR9

Shailendra Vikas[1], W. Michael Wood-Vasey[1], Britt Lundgren[2], Nicholas P. Ross[3], Adam D. Myers[4],
Yusra AlSayyad[5], Donald G. York[6,7], Donald P. Schneider[8,9], J. Brinkmann[10], Dmitry Bizyaev[10],
Howard Brewington[10], Jian Ge[11], Elena Malanushenko[10], Viktor Malanushenko[10], Demitri Muna[12],
Daniel Oravetz[10], Kaike Pan[10], Isabelle Pâris[13,14], Patrick Petitjean[13], Stephanie Snedden[10], Alaina Shelden[10],
Audrey Simmons[10], and Benjamin A. Weaver[12]

[1] Pittsburgh Particle Physics, Astrophysics, and Cosmology Center (PITT PACC), Department of Physics and Astronomy,
University of Pittsburgh, Pittsburgh, PA 15260, USA; skv4@pitt.edu
[2] Department of Physics, Yale University, New Haven, CT 06511, USA
[3] Lawrence Berkeley National Laboratory, 1 Cyclotron Road, Berkeley, CA 92420, USA
[4] Department of Physics and Astronomy, University of Wyoming, Laramie, WY 82071, USA
[5] Department of Astronomy, University of Washington, Seattle, WA 98195, USA
[6] Department of Astronomy, University of Chicago, 5640 S. Ellis Ave, Chicago, IL 60637, USA
[7] The Enrico Fermi Institute, University of Chicago, 5640 S. Ellis Ave, Chicago, IL 60637, USA
[8] Department of Astronomy and Astrophysics, The Pennsylvania State University, University Park, PA 16802, USA
[9] Institute for Gravitation and the Cosmos, The Pennsylvania State University, University Park, PA 16802, USA
[10] Apache Point Observatory, P.O. Box 59, Sunspot, NM 88349-0059, USA
[11] Department of Astronomy, University of Florida, Gainesville, FL 32611, USA
[12] Center for Cosmology and Particle Physics, New York University, New York, NY 10003, USA
[13] UPMC-CNRS, UMR7095, Institut d'Astrophysique de Paris, F-75014 Paris, France
[14] Departamento de Astronomía, Universidad de Chile, Casilla 36-D, Santiago, Chile

ABSTRACT

We measure the two-point cross-correlation function of C IV absorber systems and quasars, using spectroscopic data from the Sloan Digital Sky Survey III Baryon Oscillation Spectroscopic Survey (BOSS; Data Release 9). The 19,701 quasars and 6149 C IV "moderate" absorbers, 0.28 Å < rest-frame equivalent width (EW) < 5 Å, in our study cover a redshift range of $2.1 < z < 2.5$ over 3300 deg^2 and represent a factor of two increase in sample size over previous investigations. We find a correlation scale length and slope of the redshift-space cross-correlation function of $s_0 = 8.46 \pm 1.24$ Mpc, $\gamma = 1.68 \pm 0.19$, in the redshift-space range $10 < s < 100$ Mpc. We find a projected cross-correlation function of C IV absorption systems and quasars of $r_0 = 7.76 \pm 2.80$ Mpc, $\gamma = 1.74 \pm 0.21$. We measure the combined quasar and C IV bias to be $b_{QSO}b_{C IV} = 8.81 \pm 2.28$. Using an estimate of b_{QSO} from the quasar auto-correlation function we find $b_{C IV} = 2.38 \pm 0.62$. This $b_{C IV}$ implies that EW > 0.28 Å C IV absorbers at $z \sim 2.3$ are typically found in dark matter halos that have masses $\geqslant 10^{11.3}$–$10^{13.4}$ $M_\odot$ at that redshift. The complete BOSS sample will triple the number of both quasars and absorption systems and increase the power of this cross-correlation measurement by a factor of two.

Key words: intergalactic medium – large-scale structure of universe – quasars: absorption lines

Online-only material: color figures

1. INTRODUCTION

Understanding the formation and evolution of structure in the cosmos is fundamental to understanding the formation of galaxies and the elements. The distribution of absorption systems can provide key insights into the formation and distribution of elements in and around galaxies in the early universe.

Quasars are highly luminous objects that are believed to be supermassive black holes (Salpeter 1964; Lynden-Bell 1969) accreting material. Being very luminous, they can be seen at large distances and are therefore ideal for the study of large-scale clustering at early cosmic times. Quasars are also very useful for probing the space along the line of sight from the quasar to Earth. Intervening material absorbs photons at wavelengths characteristic of its constituent elements (e.g., C IV absorbs at 1549 Å) and causes quasar absorption lines (QALs) in spectra of background QSOs. QALs are currently thought to be from two sources: (1) gas in the host galaxy dark and (2) intervening gas in the dark matter (DM) host halos along the line of sight

to the quasar (e.g., Lynds 1971; Bergeron 1986; Sargent et al. 1988; Steidel & Sargent 1992; Steidel et al. 1994; Petitjean et al. 1994).

Among the absorbers observed near the same redshift as the quasar ($\Delta z < 0.25$), some arise from gas in the host galaxy and are likely from high-velocity winds coming from the central region (e.g., Wild et al. 2008; Nestor et al. 2008). Hence they usually appear noticeably blueshifted with respect to the quasar emission spectrum despite being physically close to the quasars.

The origin of intergalactic QAL systems is not well understood. They could be produced, for example, by (1) isolated initial generation of stars (Population III); (2) gas ejected into the intergalactic medium from proto-galaxies in merger processes (Gnedin 1998); (3) gas ejected from star-forming processes within galaxies, transported to large distances by galactic superwinds (Voit 1996; Heckman et al. 2000; Pettini et al. 2001, 2002) or jets from active galactic nuclei (Bahcall & Spitzer 1969; Mo & Miralda-Escudé 1996; Maller & Bullock 2004; Chelouche et al. 2008); (4) processes in the cold gas in DM

halos (Bahcall & Spitzer 1969; Mo & Miralda-Escudé 1996; Maller & Bullock 2004; Chelouche et al. 2008) around star-forming galaxies.

One way to differentiate between these various scenarios of metal-enrichment of the intergalactic medium is to measure the clustering strength of the QAL systems (Adelberger et al. 2005a). For example, in the simple model where QAL systems originate from Population III stars, QAL systems would be more homogeneously distributed and their correlation function would be similar to the correlation function of the DM itself. However, if the QAL gas originated in star-forming galaxies and was expelled by supernova blast waves into the intergalactic medium, we would expect the QAL systems to have a more biased correlation function matching that of star-forming galaxies. Alternatively, if the QAL systems are from quasars and expelled by outflows, we would expect the QAL systems to have a strongly biased correlation function similar to quasars. The measurement of the QAL correlation function thus enables us to relate the QAL systems to the mass of the halos in which they reside.

Improving our knowledge of the correlation strength of intervening QALs can then be used to better estimate the fraction of non-intervening QALs that are due to the quasar environment, and do not follow the clustering properties exhibited by other QAL systems. In this document, we refer to all such QAL systems as "intrinsic," making no distinction between systems that are sometimes more specifically referred to as "intrinsic" or "associated." Our definition of "intrinsic" QAL systems thus includes those with high outward velocity with respect to quasars and overlap in redshift space with the intergalactic QAL systems. Understanding the correlation of the intergalactic QAL systems will allow for more accurate measurements of the spatial and velocity distribution of the intrinsic QALs in the future, and in turn, will help constrain the astrophysics of quasars and their host galaxies.

There have been many investigations of the clustering properties of different QALs. Because most spectra are taken in optical observer-frame wavelengths, different species of QALs have usually been studied in different redshift ranges according to their rest-frame wavelength and uniqueness of identification. Mg II ($\lambda 2796$, $\lambda 2803$) and C IV ($\lambda 1548$, $\lambda 1550$) are the two most-studied species because their prominent absorption double lines make them easy to identify, they trace out significant respective regions of redshift space, and they are relatively common in optical spectra of quasars. Previous works have studied Mg II systems in a redshift range of $0.2 < z < 2$ (Petitjean & Bergeron 1990; Steidel & Sargent 1992; Churchill et al. 2003; Bouché et al. 2006; Lundgren et al. 2009). With C IV QALs we can reach the higher redshift range of $1.5 < z < 4$.

A number of efforts have been made to determine the C IV clustering strength using a variety of methods (Petitjean & Bergeron 1994; Outram et al. 2001; Adelberger et al. 2005a; Scannapieco et al. 2006; Wild et al. 2008; Tytler et al. 2009; Crighton et al. 2011). A few studies have measured the auto-correlation function for C IV and other absorbers (e.g., Scannapieco et al. 2006). The cross-correlation of C IV absorbers with quasars or galaxies was studied by Outram et al. (2001), Wild et al. (2008), Tytler et al. (2009), and Crighton et al. (2011), while Adelberger et al. (2005a) found that the cross-correlation function for C IV absorption systems and galaxies, based on ∼1000 absorbers, is similar to the correlation function of star-forming galaxies. All of these studies, however, are based upon a small number of quasars and C IV absorbers and lack the power to statistically probe the overall structure of a large volume of the universe. Therefore, they constrain clustering strength with relatively low precision.

New surveys with more uniform, accurate, and extensive data currently allow for a more precise QAL clustering analysis. The Sloan Digital Sky Survey III (SDSS-III) Baryonic Oscillation Spectroscopic Survey (BOSS; Eisenstein et al. 2011; Dawson et al. 2013) provides an excellent data set for such analysis. Data Release 9 (DR9; Ahn et al. 2012) contains high-quality spectra of ∼61,000 quasars at $z > 2.1$ (Pâris et al. 2012); this data set provides twice as many C IV QAL systems as previous C IV studies.

The ideal way to measure the clustering of C IV absorbers would be to perform an auto-correlation study of C IV absorbers. However, determining the uniformity and completeness of the back-lighting quasar sample together with the line-of-sight completeness of detecting C IV absorbers in quasar spectra is a significantly challenging project that requires future work.

In this paper, we calculate the two-point cross-correlation between the BOSS C IV absorbers and the BOSS quasars, which have a well-understood selection function (White et al. 2012), to provide a better estimate of clustering of the C IV absorbers. The BOSS quasar sample specifically targets quasars in the redshift range of $z > 2.2$ (Ross et al. 2012); thus there is a good overlap between the space of C IV absorbers ($1.5 < z < 4$) and the target redshift range of the BOSS quasar sample. Because both our sample C IV absorbers and quasars are from spectroscopic data, the redshifts of each sample are known quite accurately. Therefore, here we undertake a three-dimensional (3D) correlation study to extract the most information from our data set. In Section 2 we describe our sample of C IV absorbers, quasars and the randoms for quasars. In Section 3 we describe and motivate the analysis method for our cross-correlation study. In Section 4 we describe our results. In Section 5 we explore the systematic uncertainties of our analysis. We summarize the conclusions of our study in Section 6.

Throughout this paper we assume a flat ΛCDM cosmology of $\Omega_\Lambda = 0.74$, $\Omega_M = 0.26$, $w = -1$, and $h = 0.72$.

2. DATA

2.1. BOSS

SDSS-III uses the dedicated 2.5 m Sloan Foundation Telescope located at the Apache Point Observatory in New Mexico at an elevation of 2788 m (Gunn et al. 1998, 2006). BOSS is a spectroscopic survey undertaken within the SDSS-III program (Eisenstein et al. 2011). The BOSS instrument is an upgrade to the original SDSS-I/II spectrograph (Smee et al. 2012). In this work, we used data from SDSS DR9 (Ahn et al. 2012), which includes all the observations taken by the BOSS spectrograph prior to the summer shutdown in 2011 July.

The goal of BOSS is to determine the expansion history of the universe by measuring the baryon acoustic oscillation (BAO) feature using luminous galaxies at $z \sim 0.7$ and the Lyα forest traced by quasars (Cole et al. 2005; Eisenstein et al. 2005, 2011; McDonald et al. 2006; Dawson et al. 2013). The survey will obtain spectra for 1.5 million massive galaxies in order to measure the distance–redshift relation $d_A(z)$ and the Hubble parameter $H(z)$ with percent-level precision out to $z = 0.7$, using techniques that led to the first detection of the BAO feature (Cole et al. 2005; Eisenstein et al. 2005); the first BOSS results are given in Mehta et al. (2012), Padmanabhan et al. (2012), and Xu et al. (2012). BOSS is also extending a new method of BAO

measurement using the Lyα forest of 150,000 distant quasars at $z \simeq 2.5$ (McDonald et al. 2006; Slosar et al. 2011).

2.2. Quasars

BOSS targets quasars for studies of the Lyα forest. Maximizing the number of quasar sight lines, regardless of how the quasars are selected, is the best way to detect the baryon acoustic feature in the Lyα forest.

It was recognized early on in the survey, however, that additional science can be done with a *homogeneous* quasar sample, such as determinations of the quasar luminosity function, active black hole mass function, and auto-correlation function. Thus, to maximize the scientific output of the survey, the BOSS project decided to target half of the quasar sample using a uniform selection algorithm (Ross et al. 2012). This subset of the quasar data is known as the "CORE" sample. On average, approximately 40 fibers for quasars targets were allocated per deg² of the BOSS survey; 20 of these fibers are used for the CORE sample and another ~20 targets are from the "BONUS" sample. The BONUS sample uses targeting algorithms that incorporate all available information, even if it is heterogeneous on the sky, and is continually updated to maximize the number of quasars observed without regard to uniformity of selection. After initial experimentation with different selection algorithms (see, e.g., Kirkpatrick et al. 2011), the algorithm denoted "XDQSO" was finalized as the algorithm that defines the CORE sample for the rest of the survey. The details of the XDQSO targeting algorithm are presented in Bovy et al. (2011).

The main goal of having a separate homogeneous CORE sample is to enable statistical studies, which require understanding of the completeness of the survey. The work described in this paper is one study that is possible because of this CORE sample.

The BOSS survey targeting strategy divides the sky into "chunks." During the initial period, the targeting algorithm was held constant within each chunk and changed between chunks. After the chunk "boss12," the targeting algorithm for CORE was frozen, so the BOSS CORE sample is homogeneously selected subsequent to chunk 12, and will remain so until the end of the survey. Ross et al. (2012) provide the details of the quasar target selection and quasar sample.

For this study our C IV *absorber sample* comes from detections along lines of sight to both CORE and BONUS quasars, but our *quasar sample* for cross-correlation consists of only quasars from the CORE sample. Figure 1 shows the redshift distribution of the 37,831 quasars and 23,389 C IV absorbers in our study.

2.3. Random Catalog for Quasars

Because the CORE quasar target selection algorithm was evolving during the first year of the BOSS survey, the CORE quasar sample is not formally a uniform sample for these early data (see, e.g., White et al. 2012; Ross et al. 2012). However, we have explicitly checked each of these first 12 chunks and the targets selected by XDQSO versus the actual method used at the time have a near-complete overlap of objects. The cross-correlation results of the present study are thus insensitive to the minor differences in the early targeting methods. We therefore calculate the completeness of the CORE sample consistently and simply by assuming all objects were selected using the XDQSO targeting algorithm.

Reconstruction of the correlation function requires a random sample that is subject to the same survey effects as the quasar
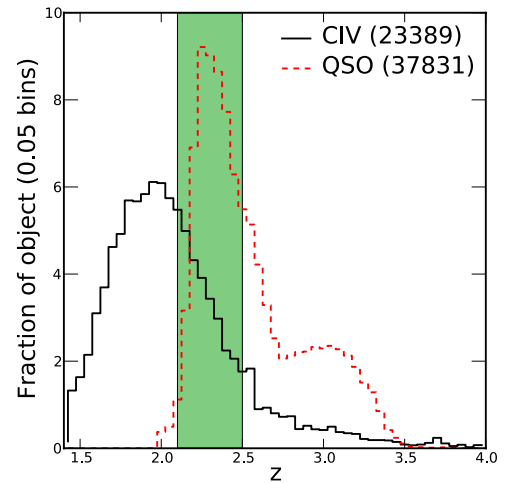

Figure 1. Redshift distribution for C IV absorbers (black, solid line) and quasars (red, dashed). While C IV absorbers come from both the CORE and BONUS samples, the quasars used in the cross-correlation are solely from the CORE DR9 sample. There are a total 37,831 quasars and 23,389 C IV absorbers in the sample. However, our clustering analysis only makes use of the 19,701 quasars and 6149 absorbers of rest-frame equivalent width >0.28 Å in the overlapping region of the distributions from $2.1 < z < 2.5$ (shaded region).

(A color version of this figure is available in the online journal.)

sample. We generated such a random sample with approximately 100 times more random points than the actual number of quasars to accurately sample the completeness in redshift and position on the sky. Therefore, the random sample represents an unclustered distribution of points following the properties of the data. The random generation, completeness mask, and redshift distribution for the CORE quasar sample are described in detail in White et al. (2012).

2.4. C IV Absorption Line Identification Pipeline

The C IV absorbers examined in this work were extracted using a modified version of the automated SDSS Data Release 7 (Abazajian et al. 2009) QAL identification pipeline described in Lundgren et al. (2009) and D. G. York et al. (in preparation). The pipeline takes as input the calibrated spectra of quasars as processed by the standard SDSS-III spectroscopic reduction pipeline (Bolton et al. 2012). It identifies absorption features by first subtracting a pseudo-continuum from each quasar. In each case, the pseudo-continuum is determined using a local smoothing window that has been found to robustly fit both the quasar emission lines and the flat regions over a broad range of quasar spectral morphologies. An algorithm is then run on the normalized spectra to identify significant absorption lines. The line-finding algorithm determines the reduced χ^2 fit to a Gaussian profile centered on each pixel of the spectrum. Errors on the equivalent width (EW) of each feature are measured directly from the error array of the quasar spectra output by the BOSS pipeline, and lines with $\geqslant 3\sigma$ significance are retained for identification. The error on the EW reflects the 1σ error on the best Gaussian fit to each absorption line, as derived from the SDSS error spectrum (photon statistics) for each object. For the rest-frame EW measurements, the observed error is then divided by $1 + z$.

The pipeline next attempts to identify each of the detected absorption features by matching ions of different species at the same redshift. The line identification algorithm operates by first identifying the most easily observable doublets, C IV

and Mg II. The search is done independently for each of these doublets, so systems that only have C IV or only have Mg II are easily found. Since absorbing gas should be physically located in the foreground of the quasar, this search is restricted to the wavelength range corresponding to a velocity of no more than 3000 km s^{-1} behind the quasar, to accommodate redshift errors in the quasar sample and motion of gas within the host halo of quasar.

Because our cross-correlation approach method does not require us to understand the completeness of our absorber sample, our study is not sensitive to C IV completeness, which can be affected by spectral artifacts such as narrow emission from night-sky lines and foreground galaxies (York et al. 2012).

For each detected doublet, an absorption redshift is determined, and the remaining unidentified absorption lines are examined for matches to other ions at the same redshift. We consider all C IV absorbers that have resolved doublets detected at $\geqslant 4\sigma$ significance.

2.5. The C IV Sample

Because the C IV absorbers in our analysis are not physically associated with the background quasars in whose spectra they are observed, our cross-correlation analysis is not affected by the selection function of the quasar sample. We thus include C IV detections from all BOSS quasars (both CORE and BONUS).

Because broad absorption lines (BALs) in quasar spectra are known to contaminate narrow absorption lines, all spectra with C IV BALs are removed from our analysis (~6.8%). The BOSS QSO catalog relies on visual examination to determine if an object is a QSO or not. BAL systems are visually identified in all cases (Pâris et al. 2012).

The full set of C IV absorbers cover the observed wavelengths 3800–7500 Å. More precisely we require

$$z_{abs} < \min\left(\sqrt{\frac{1-\beta_{min}}{1+\beta_{min}}}(1+z_{QSO})-1, \frac{7500\,\text{Å}}{1549\,\text{Å}}-1\right)$$
$$z_{abs} > \max\left(\frac{1260\,\text{Å}}{1549\,\text{Å}}(1+z_{QSO})-1, \frac{3800\,\text{Å}}{1549\,\text{Å}}-1\right), \quad (1)$$

where β is velocity in the rest frame of quasars and is defined as

$$\beta = \frac{v}{c} = \frac{(1+z_{QSO})^2 - (1+z_{abs})^2}{(1+z_{QSO})^2 + (1+z_{abs})^2}. \quad (2)$$

This range is chosen to avoid the noisy region of the spectra due to spectral contamination from sky lines at $\lambda > 7500\,\text{Å}$ and our limited ability to correct for them. We also avoid any features in the region shortward of 1260 Å in the quasar rest frame, as this region is contaminated by the N v emission line and the Lyα forest. Therefore, our cut avoids many potential false detections at the expense of missing some real systems. This approach leads to a redshift range for detectable C IV absorbers of $1.453 < z_{abs} < 3.841$.

Figure 2 shows the distribution of β for our sample. The excess of C IV absorbers in $0 < \beta < 0.02$ is due to intrinsic C IV absorbers. We remove absorbers with $\beta < 0.02$ to attempt to avoid this population. This cut decreases our C IV absorber sample to 23,339 absorbers. However, intrinsic C IV absorbers are known to contaminate the sample at much larger velocities (vanden Berk et al. 1996; Richards et al. 1999). The intrinsic absorbers may reside in the host galaxy of the quasar, the
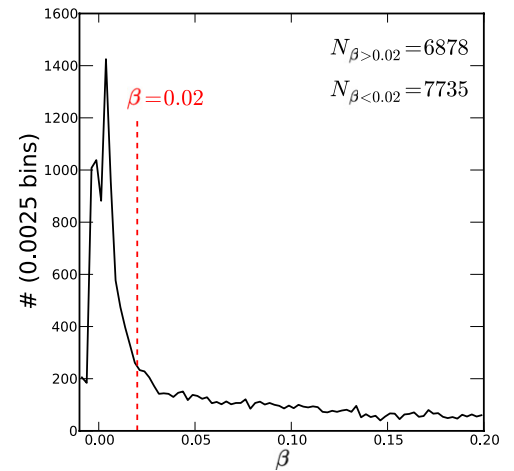

Figure 2. Distribution of β of the absorbers. The excess in the range $0.0 < \beta < 0.02$ is due to absorbers intrinsic to the quasar. The red dashed line of $\beta = 0.02$ separates the samples in our study. After the β cut, 23,389 absorbers remain.

(A color version of this figure is available in the online journal.)

gas ejected from the quasar, or within the larger clustering environment of the quasar host galaxy. The other listed sources of intrinsic C IV absorbers are eliminated by our $\beta < 0.02$ cut. Only the $\beta > 0.02$ material directly associated with the quasar can contaminate our measurement of the correlation function. Such contamination may affect the estimation of the correlation function; we estimate this effect in Section 5.4. To accurately describe the full variety of intrinsic absorbers, we would have to assume a model for the velocity distribution around the quasar. Such a study is beyond the scope of this current work and will be addressed in a future paper.

We measure the EW of the C IV doublet as the EW of the 1548 Å line. Catalog absorbers with rest-frame EWs, $W_r \geqslant 5\,\text{Å}$, can arise as artifacts of the pipeline (due to, for example, poorly subtracted night-sky lines) or from complicated blends of multiple doublets. All absorbers with such strong $W_r > 5\,\text{Å}$ features are removed from the sample. This limit removes only 15 absorbers from our sample, leaving 23,324 absorbers.

The likelihood of false positives is higher in the smallest observer-frame EW absorbers, so we apply a cut on observer-frame EW of $W_0 > 1\,\text{Å}$. Because we are not generating a random sample for the absorbers, we are more concerned about minimizing the number of false positives rather than controlling completeness. Therefore, we apply an EW cut on the observer-frame measurement. Applying this cut provides an automatic cut on rest-frame EW of $W_r > 0.28\,\text{Å}$ at our median sample redshift of $z \sim 2.3$. Figure 3 shows the distribution of absorbers in i-band magnitude and W_r space. The top panel shows the distribution of W_r for absorbers from CORE and BONUS quasars. The side panel shows the distribution of i-band magnitude for the same absorbers. After applying this cut, we are left with 20,925 absorbers.

Cross-correlating BOSS quasars and absorbers on scales out to 100 Mpc requires the two samples to be in the same redshift range ($2.1 < z \leqslant 2.5$). There are very few quasars at $z < 2.1$ and few absorbers at $z > 2.5$. This redshift range restricts our final sample to 6149 C IV absorbers (4331 from CORE lines of sight and 1818 from BONUS lines of sight), which is twice as many as Wild et al. (2008). A summary of the effects of the different cuts is given in Table 1.
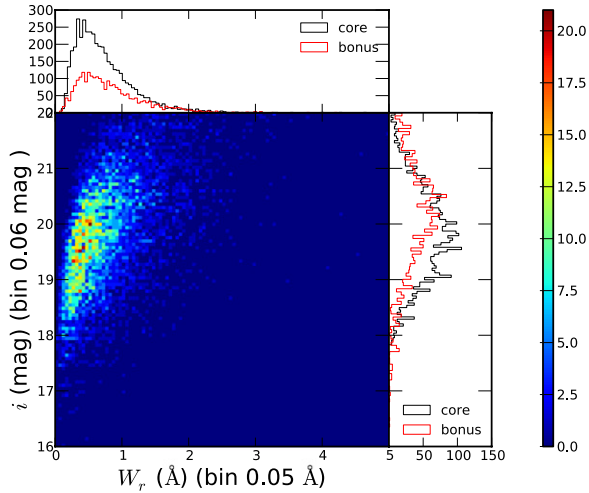
Figure 3. The bottom left panel of the plot shows the distribution of C IV absorber rest-frame equivalent width, $W_r(\text{Å})$, and the quasar i-band magnitude. The color denotes the number density of the C IV absorbers. The color bar at the right side of the plot shows the color-density scale. The lack of completeness for low W_r is evident as it is systematically more difficult to detect weaker absorbers in fainter quasars. The panel at the right shows the distribution of i-band magnitude for absorbers from the CORE and BONUS quasar samples. Similarly, the panel at the top shows the distribution of W_r for absorbers from the CORE and BONUS quasar sample.

(A color version of this figure is available in the online journal.)

Table 1
Table of $N_{\text{C IV}}$ for Different Selection Cuts

Description	$N_{\text{C IV}}$
No cut	37,441
$\beta > 0.02$	23,339
$W_r < 5\,\text{Å}$	23,324
$W_o > 1\,\text{Å}$	20,925
$2.1 < z \leqslant 2.5$	6149

3. CORRELATION ANALYSIS

The spatial correlation function, $\xi(r)$, describes the clustering of spatial points as a function of distance r. Similarly, the cross-correlation function, ξ_{A-B}, describes the clustering of two samples A and B at any given separation r. The cross-correlation function between a population of C IV absorbers and of quasars, $\xi_{\text{QSO–C IV}}(r)$, is defined as the excess probability of finding a C IV absorber at distance r from a quasar compared to the chance of a random coincidence from a homogeneous distribution:

$$dP(r) = \bar{n}_{\text{QSO}}\bar{n}_{\text{C IV}}(1 + \xi_{\text{QSO–C IV}}(r))dV_{\text{QSO}}dV_{\text{C IV}}, \quad (3)$$

where $\bar{n}_{\text{C IV}}$ is the mean density of C IV absorbers, and $\bar{n}_{\text{QSO}}$ is the mean density of quasars (Peebles 1980).

There are different estimators for the correlation function, each of which has advantages and disadvantages in the context of our study. The first method we consider is from Peebles (1980):

$$\xi_{\text{QSO–C IV}}(r) = \frac{D_{\text{C IV}}D_{\text{QSO}}}{D_{\text{C IV}}R_{\text{QSO}}} - 1, \quad (4)$$

where D_{QSO} represents our CORE sample of quasar data, R_{QSO} is the random sample that corresponds to the quasars and D_{QSO}, and $D_{\text{C IV}}$ is our C IV absorber data (which is from both CORE and BONUS). DD and DR represent the data–data and data–random pair counts as a function of r. The auto-correlation of quasars is defined in a similar manner to Equation (4). The

advantage of the estimator in Equation (4) is that it does not need a random sample for the C IV absorbers. However, while this method is simple, it is a biased estimator (Peebles 1980) as the expected estimation may not be the same as the true value of the correlation function.

The other method we consider for estimating the cross-correlation function is an unbiased estimator given by Landy & Szalay (1993):

$$\xi_{\text{QSO–C IV}}(r)$$
$$= \frac{D_{\text{C IV}}D_{\text{QSO}} - R_{\text{C IV}}D_{\text{QSO}} - D_{\text{C IV}}R_{\text{QSO}} + R_{\text{C IV}}R_{\text{QSO}}}{R_{\text{C IV}}R_{\text{QSO}}}, \quad (5)$$

where D_{QSO} and R_{QSO} are the same as in the previous equation and $D_{\text{C IV}}$ and $R_{\text{C IV}}$ are the C IV absorber sample and random sample for the C IV sample.

Equation (5) is a more robust estimator, but it would require the generation of a reliable C IV absorber random catalog. We currently lack the ability to produce such a catalog, if we want to avoid making assumptions on the redshift evolution of the density of C IV absorbers; we therefore use the Peebles estimator of Equation (4). While we use Equation (4) in this analysis, we would like to share some thoughts on Equation (5), as it will likely become the preferred method for future analyses.

The established procedure to generate random absorbers is to select a random point in the sight line to the quasar in the range that absorbers could be detected. However, this approach is not an accurate way to generate the random absorbers, as it assumes the chances of detection and number density of the absorbers to be constant along the line of sight. If the sight line covers a large enough redshift range, this assumption would affect the observed number density of absorbers. Other effects, such as gravitational lensing, may contribute to changes in the observed number density of the absorbers as well. We propose that future analyses should likely use Equation (5) with a different two-step procedure. First, a random quasar sample should be generated, which provides the locations on the sky. Second, absorbers should be assigned redshifts, drawing from the observed redshift distribution of the absorbers. This distribution may be a function of completeness of the survey. Such methods are commonly used in correlation analysis of the galaxies because of large data sets (Anderson et al. 2012; Sánchez et al. 2012; Nuza et al. 2012). This procedure would yield two advantages over our current use of Equation (4): (1) it would not have to make any assumption about the evolution of number density and probability of detection; and (2) it would reduce the effect of survey edges on the correlation function.

However, we cannot use Equation (5) because we need a larger sample of absorbers than currently available to estimate the redshift distribution for different completeness bins of quasars. At the conclusion of the BOSS survey, it will cover a large footprint with high completeness, and we will be able to generate a random sample that accurately follows the absorber population.

In addition to the 3D correlation function, we also calculate the projected cross-correlation function for the C IV absorbers and quasars. The distance between a C IV absorber and quasar can be decomposed into components perpendicular (r_p) and parallel (π) to the line of sight:

$$s^2 = r_p^2 + \pi^2. \quad (6)$$

We thus can estimate the two-dimensional cross-correlation function as

$$\xi(r_p, \pi) = \frac{D_{C\,IV}D_{QSO}(r_p, \pi)}{D_{C\,IV}R_{QSO}(r_p, \pi)} - 1 \quad (7)$$

and the projected cross-correlation function is then defined as

$$w_p(r_p) = 2 \int_0^\infty \xi(r_p, \pi)d\pi. \quad (8)$$

3.1. Error Estimation

Correlation function studies have used different methods of error estimation. These methods can be broadly placed in three categories: Poisson, Field-to-Field, and Jackknife. The Poisson error is simplest, but it assumes that the pair counts on different distant scales are independent. However, the Poisson error is known to underestimate the error at large distances, where the Poisson error is small and the cosmic variance term becomes comparable to or bigger than the Poisson error (Myers et al. 2005; Ross et al. 2007), such that the Poisson counts are correlated across different scales. In this study, we choose to use the Jackknife method, following Scranton et al. (2002).

We partition the data into 25 different areas which have roughly the same number of quasars from our random quasar catalog. We calculate 25 separate cross-correlation functions, leaving out one chunk at a time. Using the 25 cross-correlation functions, we estimate the covariance matrix from

$$\text{Cov}_{ij} = \frac{N-1}{N}\sum_{i=1}^{N}(\bar{\xi}(r_i) - \xi(r_i))(\bar{\xi}(r_j) - \xi(r_j)), \quad (9)$$

where $N = 25$ is the number of cross-correlation functions, r_i and r_j are the points where the correlation function are estimated, and $\xi(r_i)$ is the correlation function for the full sample at r_j. The diagonal element of the covariance matrix Cov_{ii} is the error estimate for the variance σ_{ii}^2 of the two-point correlation function in the ith bin.

3.2. Fitting for the Correlation Function and Bias

A standard way to model the two-point correlation function is using a power law given by

$$\xi(r) = \left(\frac{r}{r_0}\right)^{-\gamma}, \quad (10)$$

which is a good approximation for the correlation function to large distances and also a convenient form to compare with other results. The assumption of a power-law form for the correlation function in real space leads to a projected-space correlation function, defined in Equation (8), of the following form:

$$\frac{w_p}{r_p} = \left(\frac{r_0}{r_p}\right)^\gamma B\left(\frac{1}{2}, \frac{\gamma-1}{2}\right), \quad (11)$$

where $B(a, b)$ is the Euler beta function. In reality, we cannot integrate in the line-of-sight direction to infinity. If we choose to select the maximum line-of-sight distance, π_{max}, as our integration limit, we can write

$$\frac{\acute{w}_p}{r_p} = \left(\frac{r_0}{r_p}\right)^\gamma \left[B\left(\frac{1}{2}, \frac{\gamma-1}{2}\right) - B\left(\frac{r_p^2}{r_p^2 + \pi_{max}^2}; \frac{1}{2}, \frac{\gamma-1}{2}\right) \right], \quad (12)$$

Table 2
The Correlation Length and Slope for the Different Sample
of C IV Absorbers and Quasars

Description	$s_0\|r_0$ (Mpc)	γ
C IV–QSO 3D corr.	8.46 ± 1.46	1.68 ± 0.27
C IV–QSO projected corr. (r_0)	7.76 ± 2.80	1.74 ± 0.21
QSO–QSO 3D corr.	12.19 ± 0.32	1.77 ± 0.04
C IV–QSO 3D corr. ($\gamma = 1.77$)	8.92 ± 0.63	Fixed at 1.77

where $\acute{w}_p$ is the projected correlation function integrated to π_{max} and $B(z; a, b)$ is the incomplete beta function.

To fit the correlation function in the above form, we minimize

$$\chi^2 = [\xi - \hat{\xi}]^T \text{Cov}^{-1}[\xi - \hat{\xi}], \quad (13)$$

where $\hat{\xi}$ is the value from the model. However, in general, the covariance matrix is too noisy to be useful, so we only use the diagonal element of the covariance matrix.

Baryonic matter traces the gravitational potential created by DM and scales as a function of the DM halo mass (Bardeen et al. 1986; Cole & Kaiser 1989; Mo & White 1996; Sheth & Tormen 1999; Sheth et al. 2001; Jing 1998; Gao & White 2006; Tinker et al. 2010). The observed two-point correlation function of baryonic material is related to the underlying DM two-point correlation function. In the regime of linear bias (Scherrer & Weinberg 1998), we can write

$$\xi_{C\,IV-QSO}(r) = b_{C\,IV}b_{QSO}\xi_{DM}(r), \quad (14)$$

$$\xi_{QSO-QSO}(r) = b_{QSO}^2\xi_{DM}(r). \quad (15)$$

We are measuring correlations at large scales (10–100 Mpc) at moderate redshift ($z > 2$), so the linear bias approximation is quite robust. We can thus find the bias for C IV absorbers without knowing the underlying DM two-point correlation function. In terms of the other observable quantities $\xi_{QSO-QSO}$ and b_{QSO}, the C IV absorber bias is

$$b_{C\,IV} = \frac{\xi_{C\,iv-QSO}}{\xi_{QSO-QSO}}b_{QSO}. \quad (16)$$

The bias of a DM halo as a function of mass can be derived theoretically (Bardeen et al. 1986; Cole & Kaiser 1989; Mo & White 1996; Sheth & Tormen 1999; Sheth et al. 2001), but more accurate descriptions of halo bias can be derived from large-scale DM simulations (Jing 1998; Gao & White 2006; Tinker et al. 2010). Using such a calibration of DM halo bias, we can find the mass of the DM halo in which a typical C IV absorber resides.

4. RESULTS

Table 2 summarizes our measurements of the correlation length and slope for the C IV absorber and quasar correlation functions.

4.1. Cross-correlation of C IV Absorbers and Quasars

Figure 4 presents our calculated 3D cross-correlation of C IV absorbers and quasars in redshift space in the redshift range of $2.1 < z < 2.5$. Fitting the cross-correlation in the range of $10\,\text{Mpc} < s < 100$ Mpc with a power law, as described in Equation (10), we find the correlation length to
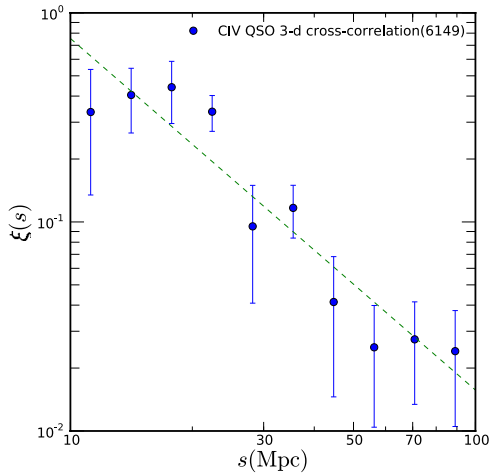
Figure 4. Cross-correlation function in redshift space for C IV absorbers and quasars from $2.1 < z < 2.5$. The dotted line is the best-fit power law, as defined in Equation (10), with $s_0 = 8.46 \pm 1.46$ Mpc and slope $\gamma = 1.68 \pm 0.27$ in the range 10 Mpc $< s <$ 100 Mpc. The horizontal axis denotes the geometric mean of the bin distance. The vertical error bar is calculated using the inverse variance weighted Jackknife method.

(A color version of this figure is available in the online journal.)

Figure 6. The correlation of r_0 and γ. The solid blue line is the 1σ contour region for a r_0 and γ fit to the 3D correlation function and the dashed red line is the same for the projected correlation function. There is a strong degeneracy between the slope and scale length of both the 3D and the projected correlation functions.

(A color version of this figure is available in the online journal.)

Figure 5. Projected correlation function for C IV absorbers and quasars. The dotted line is the best-fit power law, as defined in Equations (11) and (12), with $r_0 = 7.76 \pm 2.80$ Mpc and slope $\gamma = 1.74 \pm 0.21$ in the range 10 Mpc $< r_p <$ 100 Mpc. The horizontal axis denotes the geometric mean of projected distance bin. The redshift range for the C IV absorbers and quasars is $2.1 < z < 2.5$.

(A color version of this figure is available in the online journal.)

Figure 7. Correlation function for 10 Mpc $< s <$ 1000 Mpc with a bin size of 10 Mpc. The errors are based on a Poisson distribution of the number of pairs. The redshift range for the data is $2.1 < z < 2.5$. The blue dashed line is the best-fit power law $s_0 = 8.46 \pm 1.46$ Mpc and $\gamma = 1.68 \pm 0.27$. This power-law approximation significantly underpredicts the correlation at distances $s > 100$ Mpc and we conclude it is invalid at this scale.

(A color version of this figure is available in the online journal.)

be $s_0 = 8.46 \pm 1.46$ Mpc with a slope $\gamma = 1.68 \pm 0.27$. For the fit we found $\chi^2/\text{dof} = 10.88/8 = 1.36$, which suggests it is a quite reasonable fit to the data. However, there is significant degeneracy between the parameters s_0 and γ, as changes due to an increase in slope can be caused by the increase of correlation length. The correlation coefficient between s_0 and γ for our fit is 0.86, which suggests a high degree of correlation. The solid blue line in Figure 6 shows the contour of s_0 and γ degeneracy. We do not expect our cross-correlation measurement to be accurate in the range of $s < 10$ Mpc as at this scale we expect SDSS-III fiber collision to contaminate the astrophysical clustering signal.

Figure 5 presents the projected cross-correlation of the C IV absorbers and quasars in the same redshift range $2.1 < z < 2.5$. We fit the cross-correlation in the range of 10 Mpc $< r_p <$ 100 Mpc with a power law, as described in Equations (11) and (12). We find the best-fit power-law length to be $r_0 =$
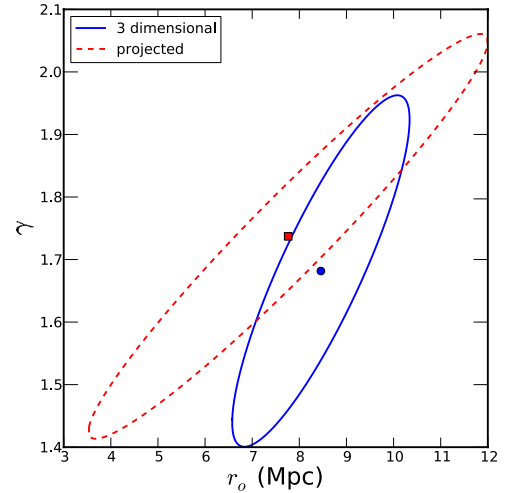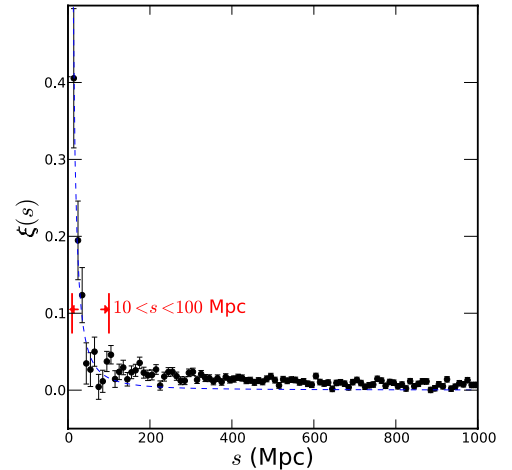
7.76 ± 2.80 Mpc with a slope $\gamma = 1.74 \pm 0.21$. We integrate the correlation function in the line-of-sight direction until $\pi_{\max} = 60$ Mpc and find a $\chi^2/\text{dof} = 9.20/8 = 1.15$. Our estimates of the length scale and power-law slope are highly degenerate indicated by a correlation coefficient of 0.96. The dashed red line in Figure 6 shows the contour of r_0 and γ degeneracy.

4.2. Cross-correlation at Large Distance

Figure 7 shows the correlation function in the range of 10 Mpc $< s <$ 1000 Mpc in bins of 10 Mpc. The errors are Poisson errors. The blue line is the best-fit cross-correlation function. We find that the power-law fit does not fit the data for distances $s > 100$ Mpc. This disagreement is not entirely unexpected as the correlation function at large distances should not necessarily be well approximated by the small-scale power

law. Both the observed and simple models for the correlation function gradually approach zero at larger distances. Cosmic variance can contribute a small offset from zero at all scales, but it is also possible that there is unknown contamination leading to an artificial excess of power on these $s > 100$ Mpc scales.

However, these features of the correlation function from 100 to 1000 Mpc do not immediately affect our main conclusions in this paper based on the correlation function measured from 10 to 100 Mpc.

4.3. Estimation of C IV Bias

In order to estimate the bias of C IV absorbers using Equation (16), we must calculate the bias for quasars, b_{QSO}. The quasar bias is given by $b_{\mathrm{QSO}}(z) = \xi_{\mathrm{QSO-QSO}}(r, z)/\xi_{\mathrm{DM}}(r, z)$, where $\xi_{\mathrm{QSO-QSO}}(r, z)$ is the real-space correlation function of our quasar sample and $\xi_{\mathrm{DM}}(r, z)$ is the theoretical matter correlation function.

A full treatment of the BOSS quasar auto-correlation from 4 to 36 Mpc is given in White et al. (2012). Our analysis here is simpler, focused on the larger scale of 10–100 Mpc, to extract a reliable quasar bias to compute the C IV absorber bias. We use the same tools for the quasar random sample and completeness map as in White et al. (2012), but while that work required a completeness of >0.75, we do not apply a completeness cut in order to use all of the C IV absorbers. Our slightly different approach in this work gains power by including more C IV absorbers and focusing on larger-scale correlations.

We follow the method adopted by Ross et al. (2009) to calculate quasar bias. We calculate the volume-average correlation function $\bar{\xi}$, defined as

$$\bar{\xi} = \frac{\int_{s_{\min}}^{s_{\max}} 4\pi \acute{s}^2 \xi(\acute{s}) d\acute{s}}{\int_{s_{\min}}^{s_{\max}} 4\pi \acute{s}^2 d\acute{s}} \qquad (17)$$

$$= \frac{3}{(s_{\max}^3 - s_{\min}^3)} \int_{s_{\min}}^{s_{\max}} \xi(\acute{s}) \acute{s}^2 d\acute{s}, \qquad (18)$$

where $s_{\min} = 10$ Mpc and $s_{\max} = 100$ Mpc for our case. The volume-average correlation function minimizes non-linear effects. While the theoretical definition of the scale-independent bias is expressed in terms of the real-space clustering, we measure the redshift-space correlation function. To minimize the error caused by this difference, we use a linear-regime relation between the redshift-space and real-space correlation function given by

$$\xi(s) = \xi(r)\left(1 + \frac{2}{3}\beta(z) + \frac{1}{5}\beta^2(z)\right), \qquad (19)$$

where

$$\beta(z) = \frac{\Omega_m^{0.55}(z)}{b(z)}. \qquad (20)$$

The difference in the real-space and redshift-space correlation functions is due to redshift distortion caused by infall of baryonic matter toward the overdensity of matter (Kaiser 1987; Fisher et al. 1994; Peacock et al. 2001; Hawkins et al. 2003; Ross et al. 2007; Guzzo et al. 2008). Using Equations (2) and (19) and the definition of bias, we find the expression for bias to be

$$b_{\mathrm{QSO}}(z) = \sqrt{\frac{\bar{\xi}_{\mathrm{QSO-QSO}}(s, z)}{\bar{\xi}_{\mathrm{DM}}(r, z)} - \frac{4\Omega_m^{1.1}(z)}{45} - \frac{\Omega_m^{0.55}(z)}{3}}, \qquad (21)$$
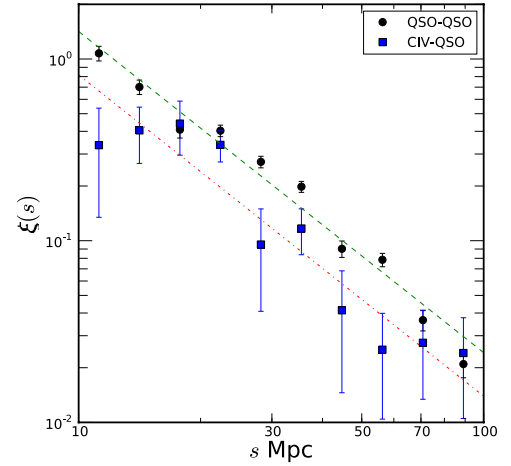

Figure 8. The quasar auto-correlation function (black circles). The green dashed line is the best power law fit in the range of $10\,\mathrm{Mpc} < s < 100\,\mathrm{Mpc}$. The redshift range for the data is $2.1 < z < 2.5$. The best-fit value for the power law is $s_0 = 12.19 \pm 0.32$ Mpc and slope $\gamma = 1.77 \pm 0.04$. The blue squares are the cross-correlation measurement for C IV absorbers and quasars over this redshift range. The red dash-dot line is the best-fit value for the correlation length, $s_0 = 8.92 \pm 0.63$ Mpc, assuming a fixed slope derived from the quasar auto-correlation.

(A color version of this figure is available in the online journal.)

where the volume-averaged $\bar{\xi}_{\mathrm{QSO-QSO}}$ is calculated from our measured $\xi_{\mathrm{QSO-QSO}}$, and $\bar{\xi}_{\mathrm{DM}}$ is calculated from the theoretical estimate of ξ_{DM}. We calculate ξ_{DM} from the model of Smith et al. (2003) for a non-linear power spectrum of DM, which is quite accurate for the distance range we are considering.

The cross-correlation suffers from redshift distortions in a similar manner as the auto-correlation. Hence the bias for cross-correlation can be given by the following:

$$\sqrt{b_{\mathrm{QSO}}b_{\mathrm{C\,IV}}} = \sqrt{\frac{\bar{\xi}_{\mathrm{C\,IV-QSO}}(s, z)}{\bar{\xi}_{\mathrm{DM}}(r, z)} - \frac{4\Omega_m^{1.1}(z)}{45} - \frac{\Omega_m^{0.55}(z)}{3}}. \qquad (22)$$

Combining Equations (21) and (22), we can calculate the bias for the C IV absorbers.

Figure 8 presents the auto-correlation function (black squares) for the BOSS DR9 quasars in the redshift range $2.1 < z < 2.5$, over the redshift-space distance range $10\,\mathrm{Mpc} < s < 100\,\mathrm{Mpc}$. The errors are calculated using the Jackknife method. We fit the quasar auto-correlation with a power law and find the correlation length to be $s_0 = 12.19 \pm 0.32$ Mpc ($8.78 \pm 0.23\,h^{-1}$ Mpc; $h = 0.72$) with a power-law slope $\gamma = 1.77 \pm 0.04$. White et al. (2012) found the correlation length $s_0 = 9.7 \pm 0.5\,h^{-1}$ Mpc for fixed slope of -2 ($\gamma = 2$) as compared to $9.52 \pm 0.13\,h^{-1}$ Mpc for our estimate using the same fixed slope.

The power-law parameters s_0 and γ are highly degenerate; higher estimates of γ lead to higher estimate of s_0 (see, e.g., Figure 6). We estimate the correlation in the range of 10–100 Mpc while White et al. (2012) performed their measurement over 3–$25\,h^{-1}$ Mpc (4.2–35.7 Mpc; $h = 0.72$).

The slope of the quasar correlation function in Figure 8 is roughly consistent with an assumption of linear bias, although the power-law model does not completely explain the data. We have not done any systematic error analysis for the QSO auto-correlation function, as the auto-correlation of quasars is not the aim of this work; we refer readers interested in this subject to White et al. (2012).

Figure 8 also shows the cross-correlation function of C IV absorbers and quasars fit with the slope of the quasar auto-correlation. The correlation length of C IV absorber-quasar in this case is $s_0 = 8.92 \pm 0.63$ Mpc. Using the method described above, we find the combined bias is $\sqrt{b_{QSO} b_{C IV}} = 2.97 \pm 0.38$. We estimate the bias for quasars to be $b_{QSO} = 3.71$. Using the b_{QSO} we determine the bias for C IV absorbers to be $b_{C IV} = 2.38 \pm 0.62$.

We use this C IV bias value to calculate the mass of the typical DM halo in which these C IV absorbers reside (see Section 3.2). Using the model described by Sheth & Tormen (1999), which provides a relationship between halo mass and the bias for a given redshift, we find that the minimum mass of the DM halo for moderate C IV absorbers ($0.28 \text{ Å} < W_r < 5 \text{ Å}$) is $M_{C IV} = 10^{12} M_\odot$ for our median redshift of $z = 2.3$. Moderate C IV absorbers are quite specifically more clustered than halos less massive than this. Because the mass function for DM halos has a steep negative slope for high-mass halos ($>10^{12} M_\odot$), if moderate C IV absorbers were found in lower-mass halos, then correspondingly greater numbers of such absorbers would have significantly diluted the correlation function we measured.

These results imply that the DM halos more massive than $10^{12} M_\odot$ contain enough C IV gas to produce an absorption feature stronger than 0.28 Å at $z \sim 2.3$. Less massive halos have less than $W_r < 0.28$ Å of C IV gas at this redshift.

We compare our estimation of clustering of C IV absorbers to the clustering of different types of galaxies at this redshift in the literature. Because most such studies do not calculate large-scale bias, we compare to other work using the estimation of correlation length of C IV absorbers as $r_{0, C IV-C IV} \simeq r_{0, C IV-QSO}^2 / r_{0, QSO-QSO} = 4.8 \pm 0.66$ Mpc. Adelberger et al. (2005b) measured the correlation length of BX galaxies to be 4.2 ± 0.5 Mpc at similar redshift ($2 < z < 2.5$) to ours, which is within 1σ of our measurement. BX galaxies are UV-selected massive galaxies which are expected to be similar in mass to luminous red galaxies. Hence we conclude that C IV absorbers appear to trace environments similar to, if not slightly more massive than, those occupied by BX galaxies. In contrast, Hickox et al. (2012) measured the correlation length of the submillimeter galaxies to be $7.7^{+1.8}_{-2.3}$ Mpc, in the redshift range of $1 < z < 3$, which is much larger than our estimate of C IV absorber systems. Hence we conclude that the C IV host halos are much smaller than host halos of submillimeter galaxies. White et al. (2012) measure the mass of the quasar host halos to be $\sim 2 \times 10^{12} \, h^{-1} \, M_\odot$, which is a few times more massive than host halos of C IV systems at a similar redshift.

We roughly estimate the stellar mass of the C IV systems using the results of Moster et al. (2010, see Figure 17 and Table 8 therein), which estimated the bias of galaxies as a function of redshift and stellar mass at that redshift. We find the stellar mass at $z \sim 2.3$ of host galaxies of C IV absorbers to be $\sim 10^{8.5}$–$10^9 \, M_\odot$.

Such low stellar mass galaxies cannot be easily seen at $z \sim 2.3$, so the C IV absorber systems could be useful as a proxy for the stellar mass of these host galaxies.

4.4. Comparison with Previous Results

There have been various previous studies of the correlations of C IV absorbers with quasars and galaxies. However, most of these studies concentrated on the correlation function at much smaller distances than our study. Wild et al. (2008) found a correlation length of $s_0 = 5.8 \pm 1.1 \, h^{-1}$ Mpc with $\gamma = 1.8$ for C IV absorbers with rest-frame $W_r > 0.3$ Å, compared to

our result of $s_0 = 6.09 \pm 0.89 \, h^{-1}$ Mpc (8.46 ± 1.46 Mpc; $h = 0.72$) with slope $\gamma = 1.68 \pm 0.27$. There is quite good agreement between these results. Our measurement more cleanly removes the intrinsic C IV absorbers for a correct measurement of correlation, whereas Wild et al. (2008) modeled the intrinsic C IV absorbers. While in theory our approach assumes less about the distribution of intrinsic absorbers, we find that in practice the choice of where we make the cut in β is the dominant systematic in our current analysis.

The clustering of C IV absorbers and Lyman break galaxies (LBGs) was measured in Adelberger et al. (2005a) and Cooke et al. (2006) for C IV absorbers with rest-frame EW > 0.4 Å. Adelberger et al. (2005a) measured the correlation length of C IV absorbers by comparing the LBG auto-correlation and LBG-C IV cross-correlation to be $r_0 \approx 5 \pm 1 \, h^{-1}$ Mpc (7 ± 1.4 Mpc; $h = 0.72$) at $z \simeq 3$. They also concluded that the C IV absorbers likely formed in these early large galaxies rather than in some more distributed environment. Our study from 10 Mpc $< r_p < 100$ Mpc is 1σ consistent with this result ($r_0 = 7.76 \pm 2.8$ Mpc). Our study covers a much larger redshift range and has significantly greater statistical power due to the larger number of absorbers.

Our results corroborate the idea that LBG and C IV absorbers, having similar clustering properties, reside in similar environments and the same DM potentials.

5. SYSTEMATIC UNCERTAINTIES

In this section we discuss potential systematic uncertainties in our measurement presented in Section 4.

5.1. North Galactic Cap versus Full Sample

We explore a potential systematic difference between the North Galactic Cap (NGC) and South Galactic Cap (SGC) data set. The NGC portion of the BOSS footprint is much larger than the SGC portion, which makes the correlation function for SGC alone very noisy. To explore possible systematic effects we therefore compare the correlation function of the full sample with the NGC sample. The SGC's data quality is worse compared to the NGC for several reasons. First, the SGC suffers much more contamination from the Milky Way compared to the NGC. Second, the SGC area is small (~ 700 deg^2) and the footprint is not smoothly contiguous. This leads to an enhancement of any edge effects on the correlation function compared to the more contiguous coverage of the NGC (~ 2600 deg^2). Third, our current understanding of other systematics is much better in the NGC than in the SGC area. All these issues with the SGC lead us to expect that the DR9 NGC data are more reliable than the SGC data.

We present in Figure 9 the 3D redshift-space correlation function for the NGC. The bottom panel compares this correlation function to the correlation function of the full sample. A power-law fit for the correlation function finds a correlation length $s_0 = 9.26 \pm 1.23$ Mpc with slope $\gamma = 2.06 \pm 0.25$ and a goodness-of-fit of $\chi^2/\text{dof} = 1.01$. The correlation between the s_0 and γ is 0.78. We also estimate, using the expression in Equation (22), that $\sqrt{b_{QSO} b_{C IV}} = 2.05 \pm 0.46$. Figure 10 shows the projected correlation function of the NGC sample. The bottom panel compares the projected correlation function to the projected correlation function of the full sample. We also fit the projected correlation function for r_0 and γ from Equation (11); we estimate $r_0 = 7.75 \pm 1.04$ Mpc and $\gamma = 1.84 \pm 0.09$ with a goodness-of-fit $\chi^2/\text{dof} = 1.25$.
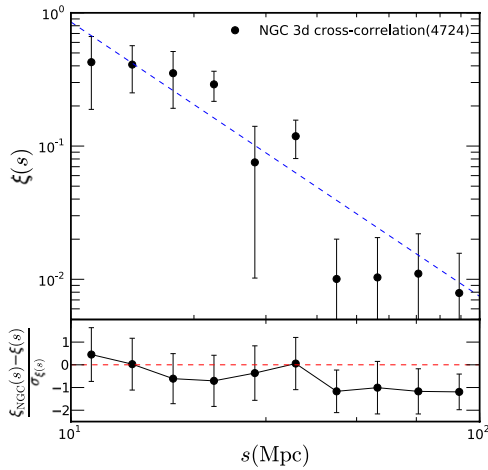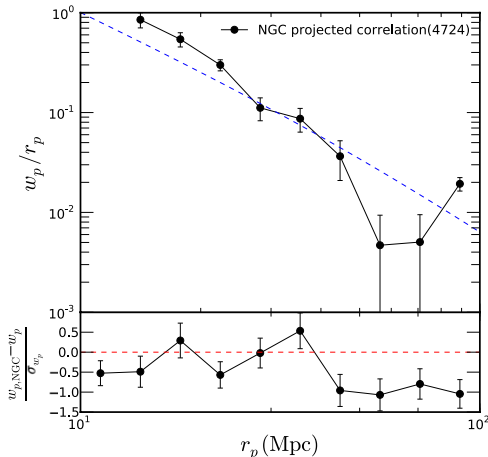
Figure 9. The redshift-space correlation function of C IV absorbers and quasars in the NGC. The dashed line is the best-fit power law, as defined in Equation (10), with $s_0 = 9.26 \pm 1.23$ Mpc and slope $\gamma = 2.06 \pm 0.25$ in the range $10 < s < 100$ Mpc. The redshift range for the C IV absorber and quasar is $2.1 < z < 2.5$. The lower panel compares the NGC correlation function to the full sample correlation function.

(A color version of this figure is available in the online journal.)

Figure 10. Projected correlation function for C IV absorbers and quasars in the NGC. The dashed line is the best-fit power law, as defined in Equation (11) and (12), with $r_0 = 7.76 \pm 2.80$ Mpc and slope $\gamma = 1.74 \pm 0.21$ in the range $10 \, \mathrm{Mpc} < w_p < 100$ Mpc in the redshift range of $2.1 < z < 2.5$. The lower panel compares the NGC projected correlation function to the full sample one.

(A color version of this figure is available in the online journal.)

From Figures 9 and 10 we see that the NGC correlation function is systematically lower than the full sample, which is also reflected in the estimation of $\sqrt{b_{QSO}b_{C\,IV}}$. White et al. (2012) also find a noticeably larger auto-correlation for the quasars at these scales in the SGC. Despite the extensive search they were unable to find any systematics which would explain the discrepancy. The excess in the quasar auto-correlation would also cause an excess in the cross-correlation measurement. The differences in the NGC and SGC cross-correlation measurements are features of the data gathered to date. However, they are 2σ consistent with each other. The sample size from the full BOSS, which will be about three times larger, will reveal whether this discrepancy is fundamental or a fluctuation.

5.2. CORE versus BONUS Systematic Error

We next explore potential systematic effects due to the survey configuration of having two separate samples of quasars: CORE
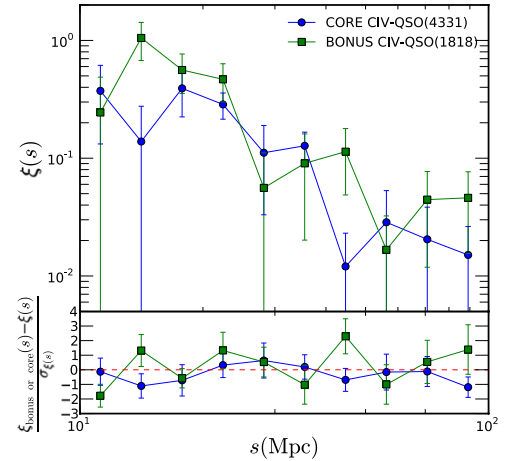

Figure 11. Cross-correlation for the CORE C IV absorbers and BONUS C IV absorbers (top panel). The two correlation functions are consistent with each other, but the large errors would mask all but very large differences. The bottom panel compares both sample correlation functions to the combined correlation function.

(A color version of this figure is available in the online journal.)

and BONUS. Because our C IV absorbers are from both CORE and BONUS quasars, we investigate differences in clustering properties of these two subsamples. Figure 11 (top panel) shows the cross-correlation measurement of the CORE C IV absorbers and BONUS C IV absorbers. The BONUS sample has only 1818 absorbers that pass our cuts; thus the error of the correlation function is quite large. It is therefore ineffective to compare the power-law fit of the two samples as the parameters are poorly constrained. As such we restrict our comparison to the correlation function to determine if the two samples are consistent. The bottom panel of Figure 11 shows the correlation functions of CORE and BONUS in comparison to the correlation function of the combined sample.

We estimate the $\sqrt{b_{QSO}b_{C\,IV}}$ for CORE and BONUS to be 2.56 ± 0.44 and 3.80 ± 0.71. Using the combined sample, the result, 2.97 ± 0.38, is within 1σ for both CORE and BONUS. Therefore, we conclude that there are no large systematic errors due to the targeting algorithm for source quasars. Any difference in the EW distribution between CORE and BONUS is also not expected to be reflected in the systematics.

5.3. Measurement Is Robust across Different BOSS Chunks

In this section we estimate the effect of the varying CORE algorithm in different chunks in the BOSS targeting process. Due to the changing targeting algorithm for the CORE sample in the first year, there could be errors introduced by estimating larger completeness in one chunk compared to other chunks because the CORE target algorithm of a different chunk selected a different fraction of the target catalog generated by the XDQSO algorithm. Within a chunk, the fractional difference in completeness determines the relative number of random points in those fields, and overall completeness only reflects in number density of the random points. In Figure 12 we compare the overall correlation function measured with the average of the 19 correlation functions, each formed from individual chunks. The error for the case when the correlation measurement is done within a chunk is the Poisson error; the overall error is calculated by adding the errors from the different chunks in quadrature. The top panel displays the correlation functions $\xi_{\mathrm{chunk}}(s)$ and $\xi(s)$. The bottom panel is the difference of the
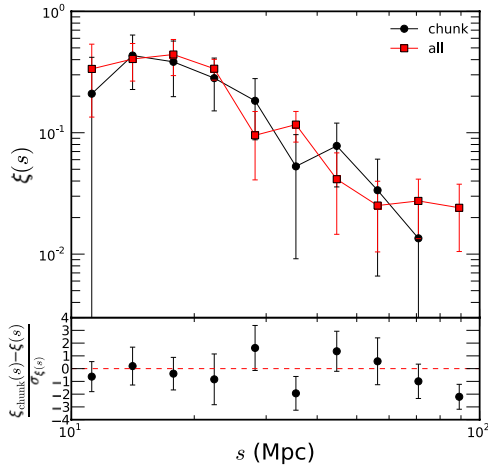
Figure 12. Top panel compares the average of cross-correlation functions calculated within chunks to the overall correlation function in the redshift distance range $10 < s < 100$ Mpc. The bottom plot is the difference of the correlation function (in units of 1σ Jackknife errors of the overall correlation function in each bin) calculated for the overall correlation function. The plots indicate no significant systematic error for the correlation function caused by different algorithms used in different chunks and hence the overall completeness of chunks is appropriate.

(A color version of this figure is available in the online journal.)

Figure 13. Error distribution for r_0 (Mpc) from 5000 binned Jackknife resamplings of the absorber sample. The distribution can be well approximated as a Gaussian (dashed blue line).

(A color version of this figure is available in the online journal.)

Table 3
Random Error Distribution for r_0, γ, and $\sqrt{b_{C\,IV}b_{QSO}}$

Parameter	Mean	Std. Dev.
δr_0	2.667	0.628
$\delta\gamma$	0.293	0.068
$\delta\sqrt{b_{C\,IV}b_{QSO}}$	0.376	0.089

correlation function calculated within chunk ξ_{chunk} and the overall correlation function in units of the Jackknife error of the overall correlation function. If there is a systematic error from the chunking process and evolving CORE algorithm, we would expect either consistently more than the correlation calculated within chunks or consistently less, caused by different overall levels of completeness, due to different algorithms used in different chunks. However, Figure 12 shows no significant trend of the ξ_{chunk} being consistently either more or less than the overall estimate of the correlation function, which indicates that is there is no large effect from the use of slightly different selection algorithms in different BOSS chunks.

For the chunk correlation function we estimate $\sqrt{b_{QSO}b_{C\,IV}} = 2.07 \pm 0.61$, but the error is larger compared to the combined sample. The correlation function does not appear to be biased compared to the combined sample. For the full BOSS sample the problem will be minimal as all subsequent chunks will use the same target selection algorithm. All the coverage will fill the space in the footprint and significantly reduce any edge effects.

5.4. Other Systematic Errors

In this section we estimate the systematic effect of various properties of the sample on the estimates of the correlation strength (r_0), the slope (γ), and the bias of C IV absorbers and quasars $\sqrt{b_{C\,IV}b_{QSO}}$. The errors on our parameters are large, and the samples are not sufficiently large to perform the typical systematic analysis in which one calculates the correlation function for a bin for each parameter space and measure the change in the correlation function in every bin. Hence, we used a Jackknife procedure because it works well on small samples. To estimate each systematic, we compared the Jackknife error caused by dividing the sample into bins based on an ordering in the given parameter to the Jackknife errors from a random division of the data into the same number of bins. Below is the specific procedure we follow.

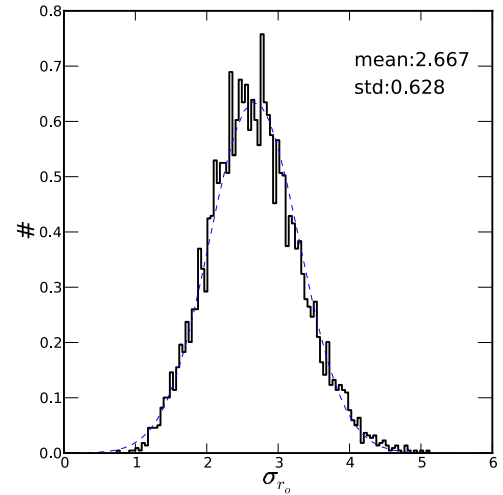1. Sort the C IV absorbers according to the given property (e.g., EW).

2. Calculate the Jackknife error on r_0, γ, and $\sqrt{b_{C\,IV}b_{QSO}}$ by dividing the C IV absorber sample into 10 bins according to the property in consideration.

3. Calculate the Jackknife error on r_0, γ, and $\sqrt{b_{C\,IV}b_{QSO}}$ by dividing the C IV absorber sample into 10 bins randomly.

4. Do the previous step 5000 times and find the distribution of r_0, γ, and $\sqrt{b_{C\,IV}b_{QSO}}$.

5. Estimate the probability of a change at least as large as the one in step 2 being drawn from the distribution of the random scatter of errors in step 4. This is known as the "p-value."

Following the above procedure, we explore the systematic effects of absorber EW, β, i-band magnitude, absorber redshift, quasar spectroscopic features, and Galactic latitude. Table 3 summarizes the mean variation and standard deviation of the parameters for each systematic. Figures 13, 14, and 15 show the distribution of the parameters r_0, γ, and $\sqrt{b_{C\,IV}b_{QSO}}$ from the random Jackknifing of the sample. Below we describe each systematic and its potential effect on the correlation function measurements. In many cases a systematic error of one property could be correlated with that of another.

1. *Absorber EW*. There are two obvious ways the EW of the C IV absorber could cause a systematic error.

   (a) There could be a few false-positive C IV absorbers in the sample, and such contamination may not be distributed uniformly across the EW distribution. The lower EW absorbers are more likely to be contaminated by false positives compared to the high equivalent absorbers. This contamination would decrease the correlation strength for lower EW absorbers.
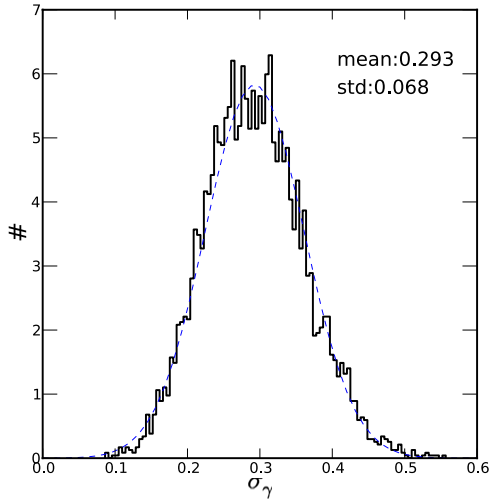
Figure 14. Error distribution for γ from 5000 binned Jackknife resamplings of the absorber sample. The distribution can be well approximated as a Gaussian (dashed blue line).
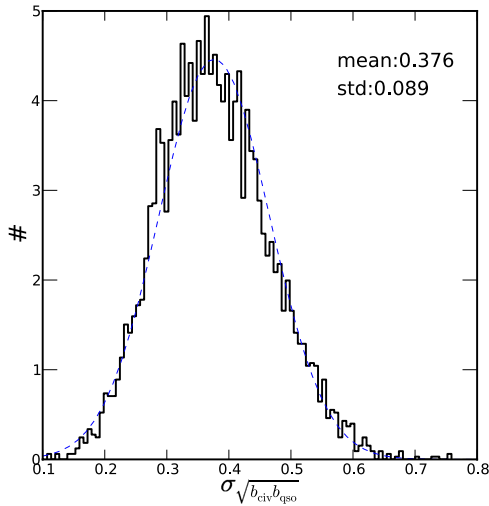(A color version of this figure is available in the online journal.)

Figure 15. Error distribution for $\sqrt{b_{C\,IV}b_{QSO}}$ from 5000 binned Jackknife resamplings of the absorber sample. The distribution can be well approximated as a Gaussian (dashed blue line).
(A color version of this figure is available in the online journal.)

(b) There could also be an intrinsic correlation dependence on EW. The higher EW absorbers could be more correlated with dark matter compared to lower EW absorbers. However, our error estimations of the correlation function are not small enough to measure this trend.

We found a potential increase in the change in $\sqrt{b_{C\,IV}b_{QSO}}$ as different EW bins are dropped with only a 13% chance (see p-value from Table 4) of such an increase in the $\sqrt{b_{C\,IV}b_{QSO}}$ distribution arising by chance.

2. β. The C IV absorber sample could have two basic origins. One may be intrinsic to quasars and quasar host galaxies, the other to intervening material in intergalactic space. These two samples will have different clustering properties. We remove a large sample of intrinsic C IV absorbers by having a minimum cut on the relative absorber velocity with respect to the quasar, β. However, we can expect some remaining contamination of the intrinsic C IV absorbers

Table 4
Systematic Error Estimates and p-values for r_0, γ, and $\sqrt{b_{C\,IV}b_{QSO}}$[a]

Description	δr_0	$\delta\gamma$	$\delta\sqrt{b_{C\,IV}b_{QSO}}$
Equivalent width	2.562(—)	0.306(0.424)	0.477(0.130)
β	3.875(0.027)	0.405(0.051)	0.424(0.298)
i-band magnitude	3.344(0.140)	0.335(0.266)	0.351(—)
Absorber redshift	2.574(—)	0.258(—)	0.412(0.346)
Galactic latitude	3.300(0.157)	0.335(0.270)	0.618(0.003)

Note. [a] Entries with probabilities too low to estimate a p-value are given as "—."

in our sample, particularly for small β where outflows dominate (see Figure 2). This contamination would be distributed asymmetrically in β because lower values of β are more likely to be contaminated by intrinsic C IV absorbers than higher β.

One other potential systematic contamination could be features in the quasar spectrum which could lead to a false-positive identification as an C IV absorber. Such false positives would reduce the estimated correlation systematically in a particular range of β.

We find that the systematic uncertainty in the choice of the β cutoff is marginally significant for $\sqrt{b_{C\,IV}b_{QSO}}$ (Table 4) and quite significant for r_0 and γ. We conclude that there is likely a small population of intrinsic C IV absorbers in our sample. We determine the error due to the β systematic alone as about $\sim$2.8 Mpc in r_0 and $\sim$0.28 in γ. The strong effect on r_0 and γ but weaker effect on $\sqrt{b_{C\,IV}b_{QSO}}$ can be explained if the intrinsic C IV affects the correlation function at small scales only (bias is determined from a volume-weighted average).

This result motivates future work to better understand the intrinsic absorber population around quasars.

3. *i-band magnitude*. There are two ways the apparent i-band magnitude can affect the correlation function systematically.

(a) False-positive C IV absorbers are more likely to occur in the spectrum of a fainter quasar than a brighter one. A false-positive signal randomly distributed would dilute any inherent clustering in the sample. Therefore, absorbers found against fainter quasars could produce systematically lower clustering strength than those found against brighter ones.

(b) The i-band magnitude could affect the correlation because brighter apparent magnitude quasars are more likely to be brighter in absolute magnitude (because of the restricted redshift range) and could be in a more highly clustered environment (Shen et al. 2013), if, for example, brighter quasars reside in more massive halos. Thus some of the intervening C IV absorbers would likely be from the clustered environment of the host galaxy.

We find this systematic error with i-band magnitude to not be significant (Table 4). The systematic effects are consistent with random errors at the 1σ and the p-value similarly indicates no significant deviation from random chance.

4. *Absorber redshift*. The potential systematic effect of contamination from false positives due to potential incomplete sky subtraction in the BOSS quasar spectra is minimal in this analysis. A sky line at a particular wavelength would

affect the C IV absorbers at a particular absorber redshift. Any sky line which falls in the observed wavelength range for a given redshift range for C IV absorbers could contribute to a reduced signal in this range. Such contamination would possibly lead to a smaller clustering measurement which would lead to systematic error. However, the strong O I sky line 5570–5590 Å is removed from the absorber pipeline, which corresponds to C IV absorber redshift of 2.59. Our cutoff absorber redshift of 2.5 avoids any neighboring part of the spectrum which might be affected. If sky lines created significant systematic problems, then one would expect to see sharp suppression in the distribution of C IV absorbers. However, Figure 1 shows no evidence for such a feature.

With this motivation in mind for potential lines we may have neglected in the above cut, we searched for a dependence of our fit parameters on the absorber redshift. However, we found no significant systematic effect (Table 4). Hence we expect that the sky subtraction for the relevant region of the spectrum is sufficient and no sky-line-contamination creates false C IV absorber detections.

5. *Galactic latitude*. The extinction through the Milky Way varies with Galactic latitude. Such extinction could be correlated to poor signal-to-noise and could lead to false-positive detection of C IV absorbers. Hence the estimate of error could be overestimating error because of contamination.

Table 4 shows the significance of the systematic error on $\sqrt{b_{\rm C\,IV}b_{\rm QSO}}$ due to Galactic latitude. This is another way of looking at the NGC versus SGC discrepancy discussed in Section 5.1. We estimate the error due to Galactic latitude on $\sqrt{b_{\rm C\,IV}b_{\rm QSO}}$ to be 0.494 with <3% probability of such a shift occurring by chance.

6. SUMMARY AND FUTURE DIRECTIONS

This study has measured the correlation strength of C IV absorbers with the quasars from the BOSS survey. We focus on correlations between $10\,\rm Mpc < s < 100\,\rm Mpc$ at $z \sim 2.3$, probing the large-scale clustering unaffected by details of the astrophysics of the galaxy environment surrounding quasars. We conclude the following.

1. The 3D two-point cross-correlation for C IV absorbers and quasars is well approximated by a power law in the distance range $10 < s < 100$ Mpc with $s_0 = 8.46 \pm 1.46$ Mpc and $\gamma = 1.68 \pm 0.27$.
2. The projected cross-correlation for C IV absorbers and quasars is well approximated by a power law in the distance range $10 < r_p < 100$ Mpc with $r_0 = 7.76 \pm 2.80$ Mpc and $\gamma = 1.74 \pm 0.21$.
3. We measure the combined QSO–C IV absorber bias $\sqrt{b_{\rm QSO}b_{\rm C\,IV}} = 2.97 \pm 0.38$.
4. We estimate the quasar auto-correlation and find a correlation length $s_0 = 12.19 \pm 0.32$ Mpc and slope $\gamma = 1.77 \pm 0.04$ and thus infer a quasar bias of $b_{\rm QSO} = 3.71$.
5. Using this estimate of the quasar bias $b_{\rm QSO}$ we find $b_{\rm C\,IV} = 2.38 \pm 0.62$ and that EW > 0.28 Å C IV absorbers reside in halos of mass $M_{\rm C\,IV} \geqslant 10^{12}\,M_\odot$.
6. The dominant sources of systematic error in our estimation of C IV absorber bias are (1) a difference as a function Galactic latitude (NGC versus SGC; Section 5.1), (2) absorber EW, and (3) potential contamination of high-velocity intrinsic absorbers ($\beta > 0.02$).

This study both lays the groundwork for subsequent improved clustering analysis with extended data sets, and enables complementary approaches to investigate C IV absorbers. With the well-constrained correlation of C IV absorbers at cosmological separations, one can propagate the two-halo correlation function down to small scales to remove this contribution from low-β absorbers, enabling a cleaner investigation of C IV absorbers in the same halo as the quasars. Any departure from the expected number of C IV absorbers would indicate the role of quasars in creating/destroying the absorbers, leading to better understanding of quasars.

A repeated analysis with the full BOSS sample will not only have ~3 times more quasars and absorbers, but will also have significantly reduced edge effects and have a more uniform completeness and coverage. The question of any NGC versus SGC difference (currently consistent with Poisson fluctuations) will be settled, and with a cleaner sample of quasars and absorbers it will be possible to make a random catalog for C IV absorbers without having to assume a specific redshift dependence of their number density. The increased number of absorbers will also allow us to measure the correlation function as a function of EW and other absorber properties. The final SDSS-III BOSS C IV absorber analysis will feature improved systematic errors and more clearly highlight the statistical power of these large samples.

REFERENCES

Abazajian, K. N., Adelman-McCarthy, J. K., Ageros, M. A., et al. 2009, ApJS, 182, 543
Adelberger, K. L., Shapley, A. E., Steidel, C. C., et al. 2005a, ApJ, 629, 636
Adelberger, K. L., Steidel, C. C., Pettini, M., et al. 2005b, ApJ, 619, 697
Ahn, C. P., Alexandroff, R., Allende Prieto, C., et al. 2012, ApJS, 203, 21
Anderson, L., Aubourg, E., Bailey, S., et al. 2012, MNRAS, 427, 3435

Bahcall, J. N., & Spitzer, L., Jr. 1969, ApJL, 156, L63
Bardeen, J. M., Bond, J. R., Kaiser, N., & Szalay, A. S. 1986, ApJ, 304, 15
Bergeron, J. 1986, A&A, 155, L8
Bolton, A. S., Schlegel, D. J., Aubourg, É., et al. 2012, AJ, 144, 144
Bouché, N., Murphy, M. T., Péroux, C., Csabai, I., & Wild, V. 2006, MNRAS, 371, 495
Bovy, J., Hennawi, J. F., Hogg, D. W., et al. 2011, ApJ, 729, 141
Chelouche, D., Ménard, B., Bowen, D. V., & Gnat, O. 2008, ApJ, 683, 55
Churchill, C. W., Vogt, S. S., & Charlton, J. C. 2003, AJ, 125, 98
Cole, S., & Kaiser, N. 1989, MNRAS, 237, 1127
Cole, S., Percival, W. J., Peacock, J. A., et al. 2005, MNRAS, 362, 505
Cooke, J., Wolfe, A. M., Gawiser, E., & Prochaska, J. X. 2006, ApJ, 652, 994
Crighton, N. H. M., Bielby, R., Shanks, T., et al. 2011, MNRAS, 414, 28
Dawson, K. S., Schlegel, D. J., Ahn, C. P., et al. 2013, AJ, 145, 10
Eisenstein, D. J., Weinberg, D. H., Agol, E., et al. 2011, AJ, 142, 72
Eisenstein, D. J., Zehavi, I., Hogg, D. W., et al. 2005, ApJ, 633, 560
Fisher, K. B., Davis, M., Strauss, M. A., Yahil, A., & Huchra, J. P. 1994, MNRAS, 267, 927
Gao, L., & White, S. D. M. 2006, MNRAS, 373, 65
Gnedin, N. Y. 1998, MNRAS, 294, 407
Gunn, J. E., Carr, M., Rockosi, C., et al. 1998, AJ, 116, 3040
Gunn, J. E., Siegmund, W. A., Mannery, E. J., et al. 2006, AJ, 131, 2332
Guzzo, L., Pierleoni, M., Meneux, B., et al. 2008, Natur, 451, 541
Hawkins, E., Maddox, S., Cole, S., et al. 2003, MNRAS, 346, 78
Heckman, T. M., Lehnert, M. D., Strickland, D. K., & Armus, L. 2000, ApJS, 129, 493
Hickox, R. C., Wardlow, J. L., Smail, I., et al. 2012, MNRAS, 421, 284
Jing, Y. P. 1998, ApJL, 503, L9
Kaiser, N. 1987, MNRAS, 227, 1
Kirkpatrick, J. A., Schlegel, D. J., Ross, N. P., et al. 2011, ApJ, 743, 125
Landy, S. D., & Szalay, A. S. 1993, ApJ, 412, 64
Lundgren, B. F., Brunner, R. J., York, D. G., et al. 2009, ApJ, 698, 819
Lynden-Bell, D. 1969, Natur, 223, 690
Lynds, R. 1971, ApJL, 164, L73
Maller, A. H., & Bullock, J. S. 2004, MNRAS, 355, 694
McDonald, P., Seljak, U., Burles, S., et al. 2006, ApJS, 163, 80
Mehta, K. T., Cuesta, A. J., Xu, X., Eisenstein, D. J., & Padmanabhan, N. 2012, MNRAS, 427, 2168
Mo, H. J., & Miralda-Escudé, J. 1996, ApJ, 469, 589
Mo, H. J., & White, S. D. M. 1996, MNRAS, 282, 347
Moster, B. P., Somerville, R. S., Maulbetsch, C., et al. 2010, ApJ, 710, 903

Myers, A. D., Outram, P. J., Shanks, T., et al. 2005, MNRAS, 359, 741
Nestor, D., Hamann, F., & Rodriguez Hidalgo, P. 2008, MNRAS, 386, 2055
Nuza, S. E., Sanchez, A. G., Prada, F., et al. 2012, arXiv:1202.6057
Outram, P. J., Smith, R. J., Shanks, T., et al. 2001, MNRAS, 328, 805
Padmanabhan, N., Xu, X., Eisenstein, D. J., et al. 2012, MNRAS, 427, 2132
Pâris, I., Petitjean, P., Aubourg, É., et al. 2012, A&A, 548, 66
Peacock, J. A., Cole, S., Norberg, P., et al. 2001, Natur, 410, 169
Peebles, P. J. E. 1980, Large-Scale Structure of the Universe (Princeton, NJ: Princeton Univ. Press)
Petitjean, P., & Bergeron, J. 1990, A&A, 231, 309
Petitjean, P., & Bergeron, J. 1994, A&A, 283, 759
Petitjean, P., Rauch, M., & Carswell, R. F. 1994, A&A, 291, 29
Pettini, M., Ellison, S. L., Bergeron, J., & Petitjean, P. 2002, A&A, 391, 21
Pettini, M., Ellison, S. L., Schaye, J., et al. 2001, Ap&SS, 277, 555
Richards, G. T., York, D. G., Yanny, B., et al. 1999, ApJ, 513, 576
Ross, N. P., da Ângela, J., Shanks, T., et al. 2007, MNRAS, 381, 573
Ross, N. P., Myers, A. D., Sheldon, E. S., et al. 2012, ApJS, 199, 3
Ross, N. P., Shen, Y., Strauss, M. A., et al. 2009, ApJ, 697, 1634
Salpeter, E. E. 1964, ApJ, 140, 796
Sánchez, A. G., Scóccola, C. G., Ross, A. J., et al. 2012, MNRAS, 425, 415
Sargent, W. L. W., Boksenberg, A., & Steidel, C. C. 1988, ApJS, 68, 539
Scannapieco, E., Pichon, C., Aracil, B., et al. 2006, MNRAS, 365, 615
Scherrer, R. J., & Weinberg, D. H. 1998, ApJ, 504, 607
Scranton, R., Johnston, D., Dodelson, S., et al. 2002, ApJ, 579, 48
Shen, Y., McBride, C., Zheng, Z., et al. 2013, AAS Meeting, 221, 307.06
Sheth, R. K., Mo, H. J., & Tormen, G. 2001, MNRAS, 323, 1
Sheth, R. K., & Tormen, G. 1999, MNRAS, 308, 119
Slosar, A., Font-Ribera, A., Pieri, M. M., et al. 2011, JCAP, 09, 001
Smee, S., Gunn, J. E., Uomoto, A., et al. 2012, arXiv:1208.2233
Smith, R. E., Peacock, J. A., Jenkins, A., et al. 2003, MNRAS, 341, 1311
Steidel, C. C., Dickinson, M., & Persson, S. E. 1994, ApJL, 437, L75
Steidel, C. C., & Sargent, W. L. W. 1992, ApJS, 80, 1
Tinker, J. L., Robertson, B. E., Kravtsov, A. V., et al. 2010, ApJ, 724, 878
Tytler, D., Gleed, M., Melis, C., et al. 2009, MNRAS, 392, 1539
vanden Berk, D. E., Quashnock, J. M., York, D. G., & Yanny, B. 1996, ApJ, 469, 78
Voit, G. M. 1996, ApJ, 465, 548
White, M., Myers, A. D., Ross, N. P., et al. 2012, MNRAS, 424, 933
Wild, V., Kauffmann, G., White, S., et al. 2008, MNRAS, 388, 227
Xu, X., Padmanabhan, N., Eisenstein, D. J., Mehta, K. T., & Cuesta, A. J. 2012, MNRAS, 427, 2146
York, D. G., Straka, L. A., Bishof, M., et al. 2012, MNRAS, 423, 3692